Applied Magnetic Resonance (2022) 53:1265–1274
https://doi.org/10.1007/s00723-021-01432-0

Applied
Magnetic Resonance

ORIGINAL PAPER

Gordon Coupler with Inductive or Capacitive Iris for Small EPR Resonators for Aqueous Samples

Richard R. Mett[1,2] · **James S. Hyde**[1]

Received: 21 July 2021 / Revised: 4 September 2021 / Accepted: 9 September 2021 /
Published online: 8 January 2022

Abstract

The Gordon coupler was introduced for use in EPR experiments at liquid helium temperatures. It provides an evanescent wave incident on the iris of a microwave resonator. Match of power incident on the coupler to the resonator is obtained by variation of the amplitude of an evanescent wave that arises from displacement of a dielectric wedge in a tapered waveguide. Reduced microphonics from helium bubbling was reported. The Gordon coupler was subsequently extended from cavity resonators to loop-gap resonators, initially at helium temperatures but later for aqueous samples. Plastics with low dielectric constants, usually Teflon, were used. Here, we extend the Gordon coupler for application in X-band five-loop–four-gap resonators using fused quartz, sapphire, or rutile dielectrics, noting that the size of the coupler can then be commensurate with dimensions of dielectric loop-gap resonators as well as dielectric tube resonators. Finite-element modeling of electromagnetic fields has been carried out, and use of a capacitive iris that interfaces with the Gordon coupler reduces pulling of the resonant frequency when matching the resonator.

1 Introduction

The Gordon coupler was introduced in 1961 [1]. The basic idea was to insert a tapered block of dielectric material into a tapered section of microwave waveguide as shown in Fig. 1. Translation of the dielectric taper along the waveguide resulted in a region that was beyond cut-off, giving rise to an evanescent wave. If the iris of a resonant cavity were interfaced with that region, coupling of power from the waveguide could be obtained. A screw arrangement permitted movement of the dielectric

✉ Richard R. Mett
rmett@mcw.edu

[1] National Biomedical EPR Center, Department of Biophysics, Medical College of Wisconsin, 8701 Watertown Plank Road, Milwaukee, WI 53226, USA

[2] Department of Physics and Chemistry, Milwaukee School of Engineering, 1025 North Broadway, Milwaukee, WI 53202, USA

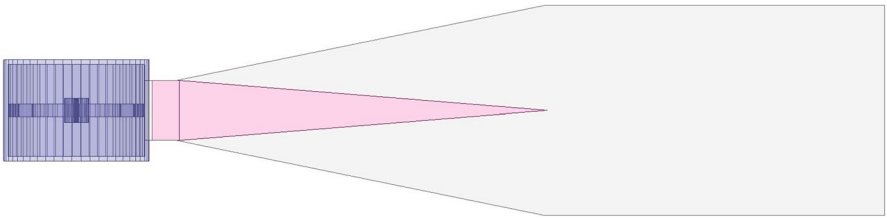

Fig. 1 Cross-sectional view, left to right, of dLGR (purple), capacitive iris, reduced-size rectangular waveguide, sapphire wedge (pink), waveguide taper, and standard WR90 waveguide. The taper length of both the wedge and waveguide is 40 mm. Other dimensions are shown in Table 2

taper to change the coupling. Additional improvements were introduced by Issacson [2] and Berlinger [3]. The structure is widely used to vary the coupling between a waveguide and a resonant microwave cavity in pulse and continuous wave EPR spectroscopy.

Froncisz and Hyde introduced the loop-gap resonator (LGR) to the field of EPR in l982 [4]. The sample was placed in a conductive one turn loop of metallic ribbon that closed on itself and was interrupted by one or two gaps. The notation one-loop–one gap, or one-loop–two-gap LGR was introduced. Since it was an ideal dipole resonator, it was placed in a cylindrical conducting shield to reduce radiation. These authors coupled microwave power to the LGR by a coaxial cable terminated by an inductive loop centered over the sample loop.

An interesting question was addressed by Britt and Klein [5]: could the Gordon coupler be used with a loop-gap resonator? They describe placement of an LGR in a microwave cavity oscillating in the rectangular TE_{102} mode and use of a Gordon coupler to introduce microwave power to the cavity. In this arrangement, the walls of the cavity serve as the radiation shield.

Other strategies were subsequently developed: Ohba et al. [6] introduced X-band microwave power from a Gordon coupler through a 3 mm diameter hole drilled in the radiation shield. Ichikawa et al. [7] increased the hole size in the radiation shield to 10×8 mm, which was so large that it could hardly be termed an iris. These authors introduced the words "distributed coupling." Gallay and van der Klink [8] placed the LGR without shield directly in the evanescent field of the Gordon coupler.

Meanwhile, Wood et al. [9] developed the three-loop–two-gap resonator. The central loop was configured for the sample, and flux returned through the outer loops. They called their structure a "controlled return flux" resonator. Radiation was greatly reduced and a radiation shield was no longer necessary. Oles et al. [10] described a distributed coupling arrangement from a Gordon coupler to one of the outer loops of this resonator.

In this paper, we continue to develop technology for use of a Gordon coupler to introduce microwave power to an LGR with an inner loop containing a single-crystal rutile dielectric resonator (DR). The hypothesis is tested that use of a conventional slotted iris between the wall of an outer loop of the five-loop–four-gap resonator [11] and the Gordon coupler becomes feasible if the dielectric constant

of the Gordon coupler is sufficiently high, see Fig. 2. In this way, dimensions of the coupler and the resonator become more commensurate. A large dielectric constant requires a small microwave waveguide, which is an advantage when coupling to small LGRs, including the dielectric loop-gap resonators (dLGRs) that currently are under development in our laboratory [12]. A further motivation for this project is that it was apparent to us that the geometry is favorable for the use of an iris with capacitive rather than inductive coupling, which previous work suggests would reduce pulling of the resonant frequency when the coupling is varied [13].

Many published papers describing Gordon couplers bring the microwave power, the matching control, and the sample entry from the top, thereby making the structures suitable for insertion into a cylindrical Dewar. In the geometry considered here, where the intent is to study aqueous samples, this compact geometry is no longer required.

Published papers show Gordon couplers that are somewhat intuitive in design. Here, we use analytic and finite element modeling of electromagnetic fields. Simple analytic equations for the TE_{10} mode are applied to the rectangular waveguide sections and the iris. Finite-element simulations were done using ANSYS High Frequency Structure Simulator (HFSS) (Canonsburg, PA) version 17.1 running on a Dell Precision Tower 7910 with dual 12 core Intel Xeon E2-2670 v.3 2.3 GHz processors with hyper-threading and 512 GB of RAM. The birefringences of the single-crystal rutile and sapphire were simulated in ANSYS HFSS by setting the appropriate values of the dielectric tensor (relative dielectric constant and loss tangent) for each of the three spatial dimensions of the crystal.

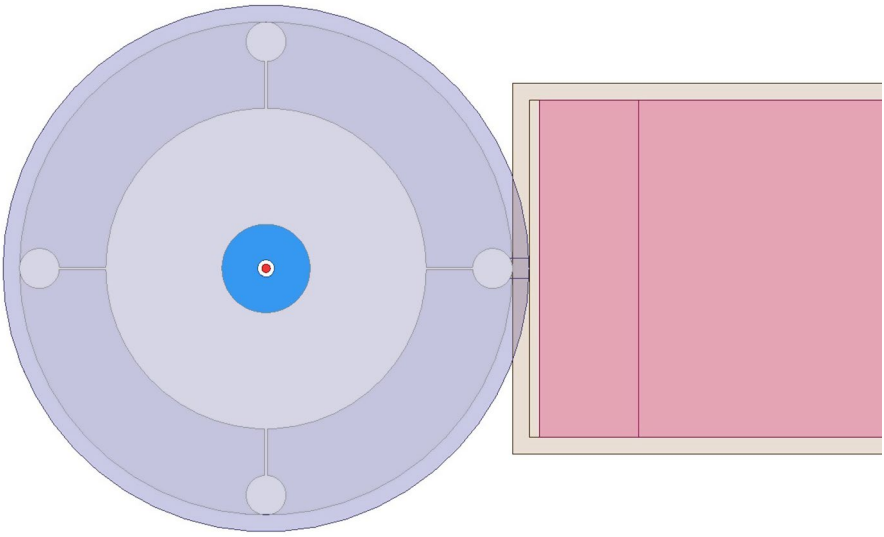

Fig. 2 Zoomed cross-sectional view from top of dLGR showing one large LGR inner loop and four small outer loops with conductor shown purple, rutile dielectric resonator blue, Teflon sample holder white, aqueous sample red, reduced-size rectangular waveguide brown, and sapphire wedge pink. Dimensions are shown in Table 2

The relative dielectric constant of single-crystal rutile is 165 parallel to the c-axis (the (001) direction) and 86 perpendicular and the loss tangent is 10^{-4} parallel to the c-axis and 8.5×10^{-5} perpendicular [14]. The relative dielectric constant of sapphire is 11.59 parallel to the c-axis and 9.40 perpendicular, and the loss tangent is 6.5×10^{-6} parallel to the c-axis and 1.8×10^{-5} perpendicular [15]. Fused quartz and Teflon were analyzed as homogeneous materials.

2 Gordon Coupler Theory

The Gordon coupler consists of four elements, shown in Fig. 1, between the resonator and the standard waveguide: an iris, a reduced-size waveguide section, a tapered waveguide section between the reduced-size section and the standard waveguide, and a moveable dielectric wedge that fills the reduced-size waveguide and is tapered down to zero at the standard waveguide. Because the TE_{10} mode propagation is independent of the short E-plane waveguide dimension, the taper of both the waveguide and wedge must occur in the long H-plane waveguide dimension. In the simplest design, the short E-plane dimension of the waveguide is constant. When the wedge is fully inserted into the reduced-size waveguide, the wedge dielectric permits the TE_{10} mode to propagate between the standard waveguide and the iris. The iris size is typically chosen under this condition to produce maximum coupling to the resonator, under conditions of minimum Q value. As the wedge is withdrawn from the reduced-size waveguide, the TE_{10} mode becomes evanescent (non-propagating, beyond cut-off) in the empty part of the reduced-size waveguide. The electric and magnetic fields in this region have an $e^{j\omega t \pm \gamma z}$ dependence [16] where ω is the radian frequency, z is the axial waveguide position, and the propagation constant

$$\gamma = \sqrt{\left(\frac{\pi}{a}\right)^2 - \left(\frac{\omega}{c}\right)^2}. \tag{1}$$

In this equation, a is the H-plane (long) waveguide dimension of the reduced-size waveguide and c is the speed of light in vacuum. This constant is real and its inverse γ^{-1} represents the axial exponential decay length of the fields. By adjusting the dimension a, γ^{-1} can be designed to produce a suitable wedge travel, e.g., 1–2 cm, that results in maximum to minimum coupling, e.g., $4\gamma^{-1} \cong 15$mm. When the wedge is inserted, the relative dielectric constant ϵ_r of the wedge material multiplies the $\left(\frac{\omega}{c}\right)^2$ term in Eq. (1). Then, γ becomes imaginary and the wavelength of the fields in the waveguide is given by $\lambda_g = \frac{2\pi}{\mathrm{Im}(\gamma)}$. The larger the dielectric constant of the wedge, the smaller the a and the smaller the γ^{-1}.

Other considerations for matching the resonator to the standard waveguide are the real wave impedance $(\frac{E}{H})$ of the TE_{10} mode in the waveguide

$$Z_{TE} = \frac{\eta}{\sqrt{\epsilon_r - \left(\frac{\lambda}{2a}\right)^2}}, \tag{2}$$

and the characteristic impedance ($\frac{V}{I}$) of the waveguide for the TE_{10} mode [17],

$$Z_0 = 2\frac{b}{a}Z_{\mathrm{TE}} \tag{3}$$

In Eq. (2), $\eta = \sqrt{\frac{\mu_0}{\epsilon_0}}$ is the wave impedance of free space and $\lambda = \frac{c}{f}$ is the free space wavelength. In Eq. (3), b is the E-plane (short) waveguide dimension. To maximize coupling between the standard waveguide and the reduced-size waveguide with the wedge in place, the Z_0 of the standard waveguide ($\epsilon_r = 1$) can be matched with the Z_0 of the reduced-size waveguide with the wedge in place. The value of this impedance is 521Ω. It follows from Eqs. (2) and (3) that when b is fixed, the characteristic impedance is matched when

$$a' = \frac{a}{\sqrt{\epsilon_r}}, \tag{4}$$

where a' is the H-plane dimension of the dielectric-filled reduced-size waveguide and a is the corresponding dimension of the standard waveguide. Table 1 shows values of various parameters that result for different dielectric materials under this impedance-matched condition. Despite the impedance match, the taper and wedge will produce a reflected TE_{10} mode [18, 19]. This was verified with the finite element simulations. When critically coupled to the resonator, the standing wave in the wedge was observed to be a larger amplitude when the reduced-sized waveguide dimension satisfied Eq. (4) than when the H-plane dimension was chosen to match the wave impedance, Eq. (2). This dimension is shown in Table 1, labeled a_w with the corresponding exponential decay lengths. Also shown in the table is the cut-off dimension a_c of the waveguide filled with the dielectric materials. At this dimension the propagation constant is zero, Eq. (1). This implies that the fields are axially uniform [20–23]. This dimension is also important for iris design as described below. The cut-off condition never appears in the taper for any wedge position.

Table 1 TE_{10} waveguide parameters at 9.5 GHz with various dielectric materials

Material	ϵ_r	a(mm)	γ^{-1}(mm)	a_w(mm)	γ^{-1}(mm)	a_c(mm)
WR90	1	22.9	–	22.9	–	15.78
Teflon	2.08	15.85	–	12.65	6.73	10.9
Fused quartz	3.78	11.76	5.61	8.74	3.34	8.12
Sapphire	11.59	6.71	2.36	4.74	1.583	4.63
Single-crystal rutile	165	1.780	0.570	1.230	0.393	1.228

3 Iris Considerations

In Ref. [13], the authors explore properties of inductive and capacitive irises used for coupling between the waveguide and loop-gap resonator. It was found that capacitive irises are preferable for several reasons including lower frequency pulling, a smaller resonator mode perturbation, and lower stored energy in the iris. In general, it was also found that an inductive iris can be characterized as a slot along the H-plane that is shorter than the cut-off dimension a_c and a capacitive iris has a corresponding slot length larger than a_c. This is because the primary electromagnetic mode in the iris can be characterized as a TE (transverse electric) mode [13]. When the iris length is close to a_c, the iris becomes resonant, which, in most situations, is undesirable because the stored energy in the iris fields becomes large.

For a Gordon coupler, it is clear that the iris length cannot be larger than the dimension of the reduced-size waveguide. For an iris not containing a dielectric, this implies that the iris is inductive, see Table 1. This fact has been corroborated by finite element simulations. Frequency pulling can be characterized in several ways including the difference between the critically matched frequency and the eigenmode resonance frequency $\Delta f = f_m - f_0$, the change in f_m with respect to Q, the change in f_m with respect to sample volume, and the change in f_m with respect to tuning adjustments. From Ref. [13], Δf is negative for an inductive iris and positive for a capacitive iris. In addition, $|\Delta f|$ is about three times smaller for a capacitive iris than an inductive iris. Because of the Lorentzian and Lorentzian-derivative LGR conductance and admittance curves as seen by the iris, all types of frequency pulling tend to be proportional to Δf. Finite-element simulations indicate that inductive irises with wedge materials fused quartz and sapphire work reasonably well with the dLGR when designed for constant wave impedance as previously described. Monotonic coupling decrease was seen with wedge distance from the iris. Quartz required about three times the wedge travel to achieve a similar coupling variation as sapphire, consistent with the values of γ^{-1} shown in Table 1. For iris dimensions 0.6 mm × 4.5 mm, the coupling factor β ranged from 6.9 to 0.68 over wedge positions 0–14.0 mm, respectively, from the iris for quartz. For the same iris size, β ranged from 6.1 to 0.66 over wedge positions 0.4–4.0 mm for sapphire. The frequency pulling $\frac{\Delta f_m}{\Delta Q}$ was found to be 2.5 kHz for quartz and 0.81 kHz for sapphire over the beta ranges given above. In both cases, the eigenmode unloaded Q was 10,200. When the sapphire wedge position was moved from 0.4 mm to 0, β increased to 30 and the frequency pulling $\frac{\Delta f_m}{\Delta Q}$ was −61 kHz over this tuning range because of the dielectric loading of the iris.

One of the goals of this work was to use a capacitive iris with the Gordon coupler. Perhaps, the simplest method of making the iris capacitive is to place dielectric in the iris slot. Rutile was found to produce insufficient coupling. However, fused quartz and sapphire were found to be practical. In choosing the iris length equal to the H-plane dimension a_w of the reduced-size waveguide, see Table 1, it was found in both cases that the electromagnetic fields in the iris were excessively large. The problem was worse for sapphire than for fused quartz. This is because a_w is relatively close to the cut-off dimension a_c as indicated in Table 1.

To reduce the problem, a can be made larger at the expense of a smaller wave impedance. For sapphire, if a is 6.5 mm, the cut-off frequency is 6.8 GHz. The wave impedance with the wedge in place is 158 Ω compared with 521 Ω for the WR90 waveguide. The mismatch causes a larger standing wave in the taper. However, adequate matching can be achieved. The exponential decay length in the empty reduced-size waveguide for $a = 6.5$ mm is $\gamma^{-1} = 2.3$ mm. For the iris and resonator parameters shown in Table 2, β monotonically decreased from 1.24 to 0.063 over the wedge travel from 0.6 mm to 4.0 mm, respectively. The frequency pulling $\frac{\Delta f_m}{\Delta Q}$ was only 0.34 kHz over this tuning range compared with 0.81 kHz for the inductive iris (as given in the previous paragraph). The electromagnetic fields in the iris and in the dLGR loop closest to the iris were also substantially smaller than for the inductive iris.

An alternative solution with a sapphire wedge is to maintain $a = 4.74$ mm, use this as the iris length, place dielectric material in the iris with $\epsilon_r = 22$, and use the constant wave impedance design. Such a material is available from TCI Ceramics, Inc. (Bethlehem, PA), an affiliate of National Magnetics Group, Inc. The presence of EPR signals would need to be investigated.

In the finite element simulations, it was noticed that if the wedge is withdrawn past the reduced-size rectangular waveguide and partly into the taper, the reduction in coupling slows. This is because as the waveguide dimension a gets larger in the taper, the exponential decay length γ^{-1}, see Eq. (1), becomes larger, increasing the required travel to produce the same attenuation. In a practical design, this is a constraint on the length of the reduced-size waveguide and the limit of the wedge travel.

Table 2 Five-loop–four-gap dLGR and coupler dimensions (mm) and properties

Description	Quantity
Sample tube id	0.25
Sample tube od	0.51
Sample volume (nL)	135
DR diameter and length	2.66
Inner loop diameter	9.66
Outer loop diameter	1.2
LGR length	1.4
Gap width	1.4
Gap thickness	0.076
Shield length	10
Iris length	6.5
Iris width	0.6
Iris thickness	0.3
Reduced-size waveguide length	3
Taper length	40
f_0(GHz)	9.5086
Q_0	6393
$\Lambda\left(\mathrm{G/W}^{1/2}\right)$	43.2

Another phenomenon noticed in the finite element simulations is that the coupling strength as a function of wedge position is monotonic for an inductive iris. Maximum coupling occurs when the wedge is against the iris. For a capacitive iris, however, this is not the case. Maximum coupling occurs when the wedge is about one iris width away from the iris. In the last few tenths of a millimeter, the coupling decreases. This is because the presence of the wedge increases the capacitance of the iris through the fringing fields near the iris. Since a larger capacitance corresponds to a smaller iris width, the coupling is decreased. This fact also provides a constraint on the wedge travel in a practical design.

4 DLGR Design

Eigenmode solutions were used to do most of the design because the solution method outputs the resonance frequency, which changes with any geometrical dimension change. Critical coupling to the waveguide is typically achieved by adjusting the iris dimensions such that the Q of the coupled resonator is half the value of the Q of the resonator with no iris (i.e., the iris filled with conductor). Once this is achieved, driven mode with a solution frequency equal to the eigenmode frequency and a narrow frequency sweep can be used to verify critical coupling. The critically matched driven solution is typically very close to the eigenmode solution in terms of frequency and fields.

The dLGR was designed with an AWG32lw Teflon sample tube (Zeus Industrial Products, Inc., Orangeburg, SC), which holds 135 nL in the 2.66 mm length of the DR. This size aqueous sample causes the unloaded eigenmode Q value of the DR to be 6393 (as shown in Table 2), about half that of the single-crystal rutile DR with no sample, 11,185. As described in Ref. [12], to achieve maximum dLGR resonator efficiency with this high Q value, the mutual inductive coupling coefficient between the DR and LGR must be made small. One way to achieve this is to increase the inner radius of the LGR, in this case to 9.66 mm. A resonator efficiency of 43.2 G/$W^{1/2}$ was achieved with the Gordon-coupled dLGR simulation as shown in Figs. 1 and 3. This is very close to the 43.9 G/$W^{1/2}$ value predicted in Ref. [12] for this sample. For this case, the behavior in terms of frequency and radiofrequency (rf) fields of the DR inside the dLGR is very close to an isolated DR. Figure 3 shows the TE_{10} mode in the WR90 waveguide propagating in from the right. The sapphire wedge concentrates the rf magnetic field as the mode travels farther into the thicker part of the wedge. The higher amplitude magnetic field at the base of the wedge and the reduced-size waveguide excites the iris and the fields in the resonator. The DR is relatively weakly mutually inductively coupled to the inner loop of the LGR and further concentrates the rf magnetic field.

The dLGR provides an ability to optimize the coupling to the DR (by changing the inner loop diameter) independently of the coupling to the iris (by changing the outer loop diameter or the number of outer loops). This three-stage coupling system permits an adjustment of the magnetic field strength near the iris independently of the iris dimensions width and length. The lower the magnetic field strength of the dLGR near the iris, the lower the coupling between the dLGR and the waveguide.

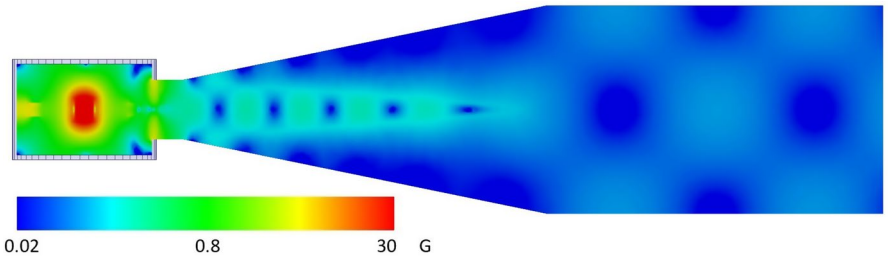

Fig. 3 Cross-sectional view of Fig. 1 except showing the magnitude of the peak rf magnetic field, red maximum to blue minimum, in a logarithmic scale. The dLGR is critically coupled with 1 W input power. The peak field in the dLGR is 86.3 G and the peak field in the WR90 is 72.3 mG. This corresponds to a resonator efficiency of 43 $G/W^{1/2}$. The single-crystal rutile DR contains a AWG32sw sample tube with 135 nL of liquid water (see Ref. [12])

Such adjustment permits the iris opening to be relatively large, which lowers the stored energy of the capacitive iris and lowers the frequency pulling while maintaining adequate coupling between the resonator and the waveguide. Higher Q values require lower stored energy around the iris compared with the resonator, and also lower coupling strength to the waveguide. The presence of the sapphire in the iris permits the iris to be capacitive, but also causes the optimum iris width to be smaller than without the dielectric.

5 Discussion

A feature of the presented Gordon coupler and dLGR design is that the entire structure from the dLGR to the standard X-band waveguide is symmetric from top to bottom with a magnetic field null along the symmetry plane. This permits the structure to be cut along this plane with no rf leakage. It permits the wedge to be supported by posts that can travel along the symmetry plane. It also permits the structure to be made in two halves and assembled. We envision the metallic outer structure being machined out of a nonconductive material such as Macor® and plated thin enough to allow modulation field penetration and thick enough to contain the rf fields. The LGR can be a metallic insert.

This work has been motivated by the hypothesis that physical displacement of a dielectric, as in a Gordon coupler, to match microwave power incident on an EPR sample resonator will result in reduced microphonics compared with use of a metallic slug or screw.

Acknowledgements It is a pleasure to dedicate this paper to Professors Klaus Moebius and Kev M. Salikhov. The careers of James S. Hyde and the honorees have continued to overlap in many ways for more than fifty years as their interests shifted gradually from physics to biophysics. Research reported in this publication was supported in part by the National Institute of General Medical Sciences of the National Institutes of Health under Award number R01GM140385. The content is solely the responsibility of the authors and does not necessarily represent the official views of the National Institutes of Health.

References

1. J.P. Gordon, Variable coupling reflection cavity for microwave spectroscopy. Rev. Sci. Instrum. **32**, 658–661 (1961)
2. R.A. Isaacson, Microwave coupler for EPR cavities at 1.3 K. Rev. Sci. Instrum. **47**, 973–974 (1976)
3. W. Berlinger, High-temperature EPR cavity for application of uniaxial stress. Rev. Sci. Instrum. **53**, 338–341 (1982)
4. W. Froncisz, J.S. Hyde, The loop-gap resonator: a new microwave lumped circuit ESR sample structure. J. Magn. Reson. **47**, 515–521 (1982)
5. R.D. Britt, M.P. Klein, A versatile loop-gap resonator probe for low-temperature electron spin-echo studies. J. Magn. Reson. **74**, 535–540 (1987)
6. Y. Ohba, C. Watanabe, S. Nakazawa, S. Yamauchi, Determination of quality factor for highly overcoupled EPR resonators. Appl. Magn. Reson. **37**, 781–794 (2010)
7. T. Ichikawa, H. Yoshida, J. Westerling, Coupling structure for the loop-gap resonator. J. Magn. Reson. **85**, 132–136 (1989)
8. R. Gallay, J.J. van der Klink, Resonator and coupling structure for spin-echo ESR. J. Phys. E Sci. Instrum. **19**, 226–230 (1986)
9. R.L. Wood, W. Froncisz, J.S. Hyde, The loop-gap resonator. II. Controlled return flux three-loop, two-gap microwave resonators for ENDOR and ESR spectroscopy. J. Magn. Reson. **58**, 243–253 (1984)
10. T. Oles, J.S. Hyde, W. Froncisz, Gordon coupler for K-band EPR loop gap resonator. Rev. Sci. Instrum. **60**, 389–391 (1989)
11. J.W. Sidabras, R.R. Mett, W. Froncisz, T.G. Camenisch, J.R. Anderson, J.S. Hyde, Multipurpose EPR loop-gap resonator and cylindrical TE_{011} cavity for aqueous samples at 94 GHz. Rev. Sci. Instrum. **78**, 034701 (2007)
12. R.R. Mett, J.W. Sidabras, J.R. Anderson, C.S. Klug, J.S. Hyde, Rutile dielectric loop-gap resonator for X-band EPR spectroscopy of small aqueous samples. J. Magn. Reson. **307**, 106585 (2019)
13. R.R. Mett, J.W. Sidabras, J.S. Hyde, Coupling of waveguide and resonator by inductive and capacitive irises for EPR spectroscopy. Appl. Magn. Reson. **35**, 285–318 (2008)
14. M.E. Tobar, J. Krupka, E.N. Ivanov, R.A. Woode, Anisotropic complex permittivity measurements of mono-crystalline rutile between 10 and 300 K. J. Appl. Phys. **83**, 1604–1609 (1998)
15. J. Krupka, K. Derzakowski, M. Tobar, J. Hartnett, R.G. Geyer, Complex permittivity of some ultralow loss dielectric crystals at cryogenic temperatures. Meas. Sci. Technol. **10**, 3887–4392 (1999)
16. S. Ramo, J.R. Whinnery, T. Van Duzer, *Fields and Waves in Communication Electronics* (Wiley, New York, 1965)
17. F.E. Goodwin, G.E. Moss, Broad-band impedance matching into dielectric-filled waveguides. IEEE Trans. Microw. Theory Tech. **11**, 36–39 (1963). https://doi.org/10.1109/TMTT.1963.1125588
18. F. Sporleder, H.-G. Unger, in *Waveguide Tapers, Transitions, and Couplers, IEE Electromagnetic Waves Series Vol. 6*. ed. by J.R. Wait, G. Millington, E.D.R. Searman (IEE, London, 1979)
19. R.R. Mett, J.W. Sidabras, J.R. Anderson, J.S. Hyde, Hyperbolic-cosine waveguide tapers and oversize rectangular waveguide for reduced broadband insertion loss in W-band electron paramagnetic resonance spectroscopy. Rev. Sci. Instrum. **82**, 074704 (2011)
20. R.R. Mett, W. Froncisz, J.S. Hyde, Axially uniform resonant cavity modes for potential use in electron paramagnetic resonance spectroscopy. Rev. Sci. Instrum. **72**, 4188–4200 (2001)
21. J.R. Anderson, R.R. Mett, J.S. Hyde, Cavities with axially uniform field for use in electron paramagnetic resonance. II. Free space generalization. Rev. Sci. Instrum. **73**, 3027–3037 (2002)
22. J.S. Hyde, R.R. Mett, J.R. Anderson, Cavities with axially uniform fields for use in electron paramagnetic resonance. III. Re-entrant geometries. Rev. Sci. Instrum. **73**, 4003–4009 (2002)
23. R.R. Mett, J.W. Sidabras, J.S. Hyde, Uniform RF fields in loop-gap resonators for EPR spectroscopy. Appl. Magn. Reson. **31**, 573–589 (2007)